International Journal of Offshore and Polar Engineering, 2017, Vol. 27, No. 4, pp. 346-356, DOI: ISOPE-17-27-4-346

Prediction of Long-Term Deformations of Offshore Wind Power Plant Foundations Using Engineer-Oriented Models Based on the High Cycle Accumulation Model

Torsten Wichtmann, Theodoros Triantafyllidis and Stylianos Chrisopoulos
Institute of Soil Mechanics and Rock Mechanics, Karlsruhe Institute of Technology
Karlsruhe, Germany

Hauke Zachert
Arcadis Deutschland GmbH
Darmstadt, Germany

The paper presents three engineer-oriented models based on the high cycle accumulation (HCA) model of Niemunis et al. [Niemunis, A., Wichmann, T., and Triantafyllidis, T. (2005) "A High Cycle Accumulation Model for Sand", *Computers and Geotechnics*, 32(4), 245-263], dedicated to the prediction of long-term deformations of offshore wind power plant (OWPP) foundations caused by wind and wave action. A sublayering model for shallow foundations under vertical cyclic loading and two different approaches (a sublayering model and a stiffness-degradation model) for monopile foundations subjected to horizontal cyclic loading are presented. The results of these models are compared to the solution from 2-D or 3-D finite element simulations with the original HCA model. Furthermore, the prediction is confronted with the prognosis of other engineer-oriented models proposed for OWPP foundations in the literature. Finally, a simplified procedure for the determination of the HCA material constants is briefly explained.

KEY WORDS: Offshore wind power plant foundations, high-cyclic loading, cumulative deformations, HCA model, engineer-oriented models, shallow foundations, monopiles.

INTRODUCTION

The cyclic loading of offshore wind power plant (OWPP) foundations due to wind and wave action leads to permanent deformations. They may endanger serviceability since the OWPP generators tolerate only a small tilting (0.5°-1°) of the tower. Therefore, an accurate prediction of these long-term deformations is indispensable. The high-cycle accumulation (HCA) model proposed by Niemunis et al. (2005) is a suitable tool for that purpose. It has been validated based on simulations of model tests and full-scale in situ tests (Hartwig, 2010; Zachert, 2015; Zachert et al., 2014, 2015, 2016). Up to now, the HCA model has been primarily applied in finite element (FE) simulations (e.g., Wichtmann et al. (2010a); Zachert et al. (2014, 2015, 2016)). Such calculations usually demand a rather laborious 3-D model and experienced knowledge on the field of FE. To facilitate the practical application of the HCA model to OWPP foundations, several simplified engineer-oriented models for different types of foundation structures have recently been developed by the authors based on the HCA equations:

- A sublayering model for the subgrade of shallow foundations under cyclic vertical loading. For example, such loading conditions are relevant for OWPPs founded on three or four separate footings. The calculation procedure using this model is similar to that in a conventional settlement calculation for foundations subjected to static loading, but with the HCA equations predicting the additional cumulative portion of settlement. In comparison to simple settlement formulas of type $s(N) = s(N = 1) \cdot f(N)$ (or similar) (Diyaljee and Raymond, 1982; Hettler, 1984; Mallwitz and Holzlöhner, 1996), sublayering models are advantageous since they can be calibrated based on element tests in the laboratory. They are also more flexible with respect to stratified ground. Furthermore, it can be demonstrated that the common settlement formulas for cyclically loaded foundations are inconsistent, since the prediction depends on which cycle is regarded as the first one (Niemunis and Wichtmann, 2014).
- A sublayering model for the soil surrounding monopile foundations under horizontal cyclic loading. The soil stiffness and the cumulative deformations are represented by springs and dashpots, respectively. The cumulative deformations are calculated with the HCA model.
- A stiffness-degradation model (SDM) for monopile foundations under horizontal cyclic loading, with the stiffness-reduction factor based on the HCA model.

The following sections present the basic ideas and equations of these engineer-oriented models, along with some exemplary cal-

culations. The predictions of the simplified models are compared to the results from FE simulations using the full HCA model.

In the case of monopile foundations, the prediction is also compared to the prognosis of the following engineer-oriented models available in the literature:

- The procedure according to the API (American Petroleum Institute, 2000) utilizing p-y curves with a reduction of the bedding stiffness considering cyclic loading.
- A modification of the API approach proposed by Dührkop (2010), based on small-scale model tests on monopiles under horizontal cyclic loading.
- The enhanced strain wedge model (ESWM) published by Taşan (2012), an extension of the strain wedge model of Norris (1986) and Ashour et al. (1998) for cyclic loading conditions.
- The SDM of Achmus et al. (2008). Using that model, a monotonic loading of the monopile is simulated with a 3D FE model and a simple elastoplastic constitutive model. Young's modulus is reduced, accounting for the increased deformations due to cyclic loading.

A critical assessment of these various models can be found in Westermann et al. (2014a,b). Simple formulas of type $y(N) = y(N = 1) \cdot f(N)$ (or similar) have been also proposed for the cumulative horizontal displacements of monopile foundations (Hettler, 1984; Leblanc et al., 2010). Unfortunately, they show the same deficits as those dedicated to shallow foundations.

A simplified procedure for the determination of the HCA model parameters further facilitates the application of the HCA model in practice. Following that procedure, all, or at least parts, of the parameters can be estimated based on granulometry or simple index tests. Therefore, the number of sophisticated and elaborate cyclic tests necessary for a calibration of the model can be significantly reduced.

SUBLAYERING MODEL FOR SHALLOW FOUNDATIONS UNDER VERTICAL CYCLIC LOADING

Basic Idea, Equations, and Calculation Procedure

The procedure is similar to a conventional settlement prediction under static loading. The subsoil is divided into several layers (Fig. 1). The sum of the accumulated deformations calculated for the individual layers represents the cumulative settlement of the foundation.

As in the FE simulations with the HCA model, the implicit and explicit parts of the calculation are distinguished from each other (Fig. 2). The implicit part comprises the loading of the foundation toward the average stress σ_F^{av} and the first so-called irregular cycle with an amplitude σ_F^{ampl}. This cycle is called irregular because it usually generates a much larger permanent deformation than subsequent cycles. The implicit steps are treated with a conventional constitutive model. In the case of this engineer-oriented approach a simple elastic model is used. All subsequent regular cycles with the same amplitude σ_F^{ampl} are handled with the HCA model. During that phase of the calculation, the increase of the cumulative deformations with the number of cycles N is predicted directly, without following the stress or strain paths within the individual cycles. The load applied to the foundation is kept constant during the explicit phase (Fig. 2).

The calculation procedure during the implicit parts can be summarized as follows:

1. The initial effective stress due to the soil's own weight (vertical component σ_{10}, horizontal one $\sigma_{30} = K_0\sigma_{10}$) is calculated in each layer.

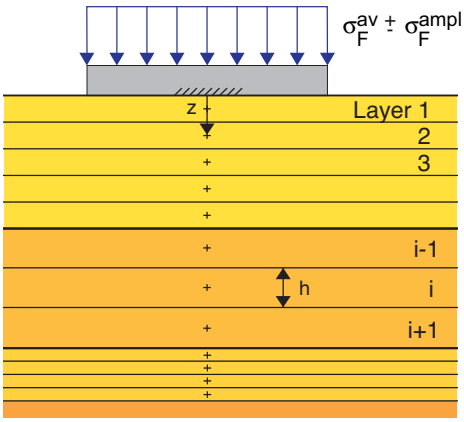

Fig. 1 Discretization of the soil into layers

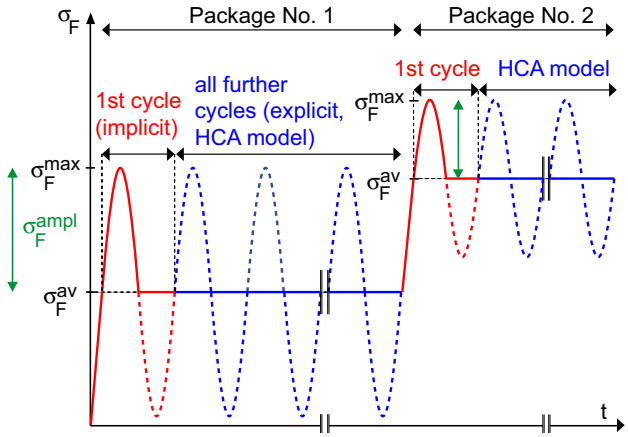

Fig. 2 Scheme of the cyclic loading applied to the foundation during two successive packages of cycles with different average stresses and stress amplitudes

2. The additional vertical ($\Delta\sigma_1^{\mathrm{av}}$) and horizontal ($\Delta\sigma_3^{\mathrm{av}} = K_0\Delta\sigma_1^{\mathrm{av}}$) stresses in the soil due to the average stress σ_F^{av} applied to the foundation are determined, using, e.g., Steinbrenner's solution for a rectangular loaded area on an elastic half-space, $\Delta\sigma_1^{\mathrm{av}} = i_R\sigma_F^{\mathrm{av}}$, with the factor i_R depending on geometry and depth (i.e., a/b and z/b). Flexible and rigid foundations are distinguished from each other. In the case of flexible foundations, the stresses are calculated for the center point, while the characteristic point is used for rigid ones.

3. The stress amplitudes σ_1^{ampl} and σ_3^{ampl} due to the amplitude σ_F^{ampl} of the cyclic loading applied to the foundation are analogously obtained. Next the maximum stresses during the cycles can be determined (e.g., $\sigma_1^{\max} = \sigma_{10} + \Delta\sigma_1^{\mathrm{av}} + \sigma_1^{\mathrm{ampl}}$).

4. The settlement caused by the first loading to the maximum stress $\sigma_F^{\max} = \sigma_F^{\mathrm{av}} + \sigma_F^{\mathrm{ampl}}$ is calculated using a pressure- and density-dependent stiffness $E_1(p, I_D)$ for the soil derived from the first loading curve in either an oedometric test (compression index C_c) or a drained triaxial test (Young's modulus E_{50} obtained from the initial phase of the $q(\varepsilon_1)$ curve), with relative density index $I_D = (e_{\max} - e)/(e_{\max} - e_{\min})$, mean pressure $p = (\sigma_1 + 2\sigma_3)/3$, and deviatoric stress $q = \sigma_1 - \sigma_3$. This part of the procedure is almost identical to a conventional

prediction of the settlement due to monotonic loading, with the only exception being that the loading is applied in a certain number of increments in order to consider nonlinearity, i.e.,

$$\Delta\varepsilon_{1,j} = \frac{\Delta\sigma_{1,j}}{E_1(p, I_D)} \qquad \varepsilon_1 = \sum \Delta\varepsilon_{1,j} \qquad \Delta h = \varepsilon_1 h_0 \quad (1)$$

with the settlement of the layer Δh and its initial height h_0. The index j numbers the time increments.

Regarding the strains in both horizontal directions, three different approaches have been implemented into the sublayering model: oedometric conditions with totally prevented lateral strains, triaxial conditions with unhindered lateral deformations, and mixed boundary conditions with partially prevented strains. Furthermore, the lateral strains depend on the geometry of the foundation (e.g. ε_3 = 0 in the case of strip foundations). For reasons of simplicity, following Nübel et al. (1999) the 3-D case is reduced to an axisymmetric one, introducing the lateral strain ratio ϑ:

$$\varepsilon_2 \quad = \quad \varepsilon_3 \; = \; \vartheta \, \varepsilon_1 \quad (2)$$

The equation of linear elasticitiy then leads to

$$\sigma_1 = \frac{E}{1+\nu}\left(\varepsilon_1 + \frac{\nu}{1-2\nu}\varepsilon_v\right) = \underbrace{E\,\frac{1-\nu+2\nu\vartheta}{(1+\nu)(1-2\nu)}}_{E_1}\,\varepsilon_1 \quad (3)$$

with Poisson's ratio ν and volumetric strain $\varepsilon_v = \varepsilon_1 + \varepsilon_2 + \varepsilon_3 = (1+2\vartheta)\varepsilon_1$. For the oedometric case (ϑ = 0), Eq. 3 delivers the conventional oedometric stiffness M (i.e., $E_1 = M = E\,\frac{1-\nu}{(1+\nu)(1-2\nu)}$), while the triaxial case ($\vartheta = -\nu$) leads to Young's modulus $E_1 = E$.

For partially constrained lateral strains (something between the oedometric and triaxial case) the factor ϑ proposed by Nübel et al. (1999) based on FE simulations is used, considering a variation with depth and a dependence on the foundation geometry (blue dashed curves in Fig. 3):

$$\vartheta(z,\alpha) = \begin{cases} \vartheta_{\infty,\mathrm{R}}\,\frac{|z|}{2b} & \text{for } \frac{|z|}{2b} \le 1 \\ \vartheta_{\infty,\mathrm{R}} & \text{for } \frac{|z|}{2b} > 1 \end{cases} \quad (4)$$

Equation 4 describes oedometric conditions ($\vartheta = 0$) directly below the foundation (z = 0), a linear increase of ϑ with depth up to $z = 2b$, and a constant ϑ at larger depths. For the axisymmetric case of a circular foundation, the maximum value $\vartheta_{\infty,R}$ is set to -0.3, while -0.2 is used for the plane strain case of a strip foundation (Nübel et al., 1999). For a rectangular foundation with dimensions $a \times b$, the value of $\vartheta_{\infty,R}$ is interpolated between both cases:

$$\vartheta_{\infty,R} \quad = \quad -\sqrt{(0.2\,\cos\alpha)^2 + (0.3\,\sin\alpha)^2} \quad (5)$$

with

$$\alpha[\mathrm{rad}] \quad = \quad \frac{b}{a}\,\frac{\pi}{2} \quad \text{and} \quad a \ge b \quad (6)$$

A circular foundation is treated equivalently to a square foundation ($a = b$) with $\alpha = \pi/2$. In the case of the strip foundation ($a \to \infty$), one obtains $\alpha = 0$.

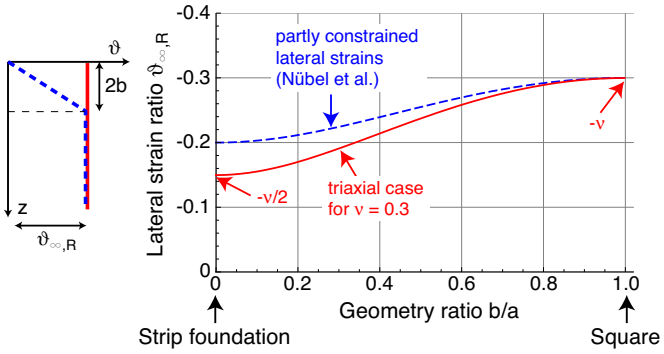

Fig. 3 Lateral strain ratio $\vartheta(z,\alpha)$ as a function of depth z (left-hand side) and in dependence on the geometry factor b/a of the foundation

To consider the foundation geometry in the triaxial case, the equations of Nübel et al. (1999) have been adapted, using a constant value of ϑ over depth (red solid curves in Fig. 3, plotted for ν = 0.3):

$$\vartheta(\alpha) \quad = \quad \vartheta_{\infty,R} = -\sqrt{(\nu/2\,\cos\alpha)^2 + (\nu\,\sin\alpha)^2} \quad (7)$$

For a square or circular foundation, one thus obtains $\vartheta(\alpha = \pi/2) = -\nu$. A strip foundation (one should speak of biaxial rather than triaxial conditions in that case) is described by $\vartheta(\alpha = 0) = -\nu/2$, i.e., an average value considering $\varepsilon_3 = 0$ and $\varepsilon_2 = -\nu\varepsilon_1$.

5. The heave due to the unloading of the foundation from $\sigma_F^{\max}$ to σ_F^{av} is analogously estimated using a p- and I_D-dependent stiffness gathered from the unloading curve in either an oedometric test (swelling index C_s) or a drained triaxial test (un- and reloading Young's modulus E_{ur}). This calculation is also done in increments. The second half of the first cycle (unloading to $\sigma_F^{\min}$ and subsequent reloading to σ_F^{av}) is not simulated since it does not generate any permanent deformations and does also not deliver any additional information necessary for the further calculation.

The calculation procedure during the explicit parts is as follows:

1. In each layer, the strain amplitude $\varepsilon^{\mathrm{ampl}}$ is calculated from

$$\varepsilon^{\mathrm{ampl}}(\vartheta) \quad = \quad \sqrt{1+2\vartheta^2}\;\varepsilon_1^{\mathrm{ampl}} \quad (8)$$

using $\varepsilon_2^{\mathrm{ampl}} = \varepsilon_3^{\mathrm{ampl}} = \vartheta\;\varepsilon_1^{\mathrm{ampl}}$. The amplitude of vertical strain $\varepsilon_1^{\mathrm{ampl}}$ is obtained from the stress amplitude σ_1^{ampl} using a secant stiffness $E_{1,\mathrm{sec}}(\vartheta)$ derived from a cyclic test (resonant column or cyclic triaxial test):

$$\varepsilon_1^{\mathrm{ampl}} \quad = \quad \sigma_1^{\mathrm{ampl}}/E_{1,\mathrm{sec}}(\vartheta) \quad (9)$$

If the well-known decrease of $E_{1,\mathrm{sec}}$ with increasing strain amplitude $\varepsilon_1^{\mathrm{ampl}}$ shall be considered, an iterative procedure is necessary in order to determine $\varepsilon_1^{\mathrm{ampl}}$.

2. The increase of the cumulative vertical strain with increasing number of cycles is calculated with the HCA model in each

layer. The following axisymmetric formulation of the HCA model is applied:

$$\begin{bmatrix}\dot{\sigma}_1\\ \dot{\sigma}_3\end{bmatrix} = \frac{E}{(1+\nu)(1-2\nu)}\begin{bmatrix}1-\nu & 2\nu\\ \nu & 1\end{bmatrix}\begin{bmatrix}\dot{\varepsilon}_1-\dot{\varepsilon}^{\text{acc}}\,m_1\\ \dot{\varepsilon}_3-\dot{\varepsilon}^{\text{acc}}\,m_3\end{bmatrix} \quad (10)$$

with $\dot{\varepsilon}_3 = \vartheta\dot{\varepsilon}_1$. In the context of HCA models, a dot over a symbol means a derivative with respect to the number of cycles N (instead of time t), i.e., $\dot{\sqcup} = \partial \sqcup / \partial N$. The components of the flow rule are adopted from the modified Cam Clay model:

$$\begin{bmatrix} m_1\\ m_3\end{bmatrix} = f\begin{bmatrix} 1/3\left(1-(\eta^{\text{av}})^2/M^2\right)+2(\eta^{\text{av}})/M^2\\ 1/3\left(1-(\eta^{\text{av}})^2/M^2\right)-(\eta^{\text{av}})/M^2\end{bmatrix} \quad (11)$$

with average stress ratio $\eta^{\text{av}} = q^{\text{av}}/p^{\text{av}}$, critical stress ratio M, and

$$f = \left[1/3\left(1-(\eta^{\text{av}})^2/M^2\right)^2+6\left(\eta^{\text{av}}/M^2\right)^2\right]^{-0.5} \quad (12)$$

The intensity of accumulation $\dot{\varepsilon}^{\text{acc}}$ entering Eq. 10 is obtained from Eq. 13:

$$\dot{\varepsilon}^{\text{acc}} = f_{\text{ampl}}\,\dot{f}_N\,f_e\,f_p\,f_Y \quad (13)$$

with the functions summarized in Table 1. The strain amplitude determined in the preceding step enters f_{ampl}.

Since the external loading on the foundation is kept constant during the explicit calculation, $\dot{\sigma}_1 = 0$ holds. The first row of Eq. 10 then delivers

$$\dot{\varepsilon}_1(\vartheta) = \left[\frac{1-\nu}{1-\nu+2\nu\vartheta}\,m_1+\frac{2\nu}{1-\nu+2\nu\vartheta}\,m_3\right]\dot{\varepsilon}^{\text{acc}} \quad (14)$$

For oedometric conditions ($\vartheta = 0$), Eq. 14 simplifies to

$$\dot{\varepsilon}_1 = \dot{\varepsilon}^{\text{acc}}\left(m_1+\frac{2\nu}{1-\nu}m_3\right) \quad (15)$$

and the second row of Eq. 10 predicts a change of the average lateral stress due to the cycles according to

$$\dot{\sigma}_3 = -\frac{E}{1-\nu}\,\dot{\varepsilon}^{\text{acc}}\,m_3 \quad (16)$$

which is, however, neglected in the model for reasons of simplicity. Setting $\dot{\sigma}_3 = 0$ in the second row of Eq. 10, one obtains the axial strain rate for triaxial conditions ($\vartheta = -\nu$):

$$\dot{\varepsilon}_1 = \dot{\varepsilon}^{\text{acc}}m_1 \quad (17)$$

The calculation of the cumulative vertical strain caused by N cycles within a layer is performed incrementally. Considering an increment of the number of cycles ΔN, the resulting increment of cumulative vertical strain is obtained from $\Delta\varepsilon_1 = \dot{\varepsilon}_1\Delta N$. The void ratio entering the function f_e in Table 1 is continuously updated during this incremental calculation. The final residual strain is multiplied by the initial height of the layer in order to obtain its settlement. A summation over all layers leads to the cumulative settlement of the foundation (see Eq. (1)).

Influencing parameter	Function	Mat. const.
Strain amplitude	$f_{\text{ampl}} = \left(\frac{\varepsilon^{\text{ampl}}}{10^{-4}}\right)^{C_{\text{ampl}}} \le 10^{C_{\text{ampl}}}$	C_{ampl}
Cyclic preloading	$\dot{f}_N = \dot{f}_N^A + \dot{f}_N^B$	C_{N1}
	$\dot{f}_N^A = C_{N1}C_{N2}\exp\left[-\frac{g^A}{C_{N1}f_{\text{ampl}}}\right]$	C_{N2}
	$\dot{f}_N^B = C_{N1}C_{N3}$	C_{N3}
Mean pressure	$f_p = \exp\left[-C_p\left(\frac{p^{\text{av}}}{100\text{ kPa}}-1\right)\right]$	C_p
Stress ratio	$f_Y = \exp\left(C_Y\,\bar{Y}^{\text{av}}\right)$	C_Y
Void ratio	$f_e = \frac{(C_e-e)^2}{1+e}\,\frac{1+e_{\max}}{(C_e-e_{\max})^2}$	C_e

Table 1 Summary of the functions and material constants of the HCA model

The total settlement of the foundation is obtained as the sum of the portion resulting from the implicit phase of the calculation (i.e., caused by the application of the average load and the first cycle) and the additional cumulative portion stemming from the explicit phase. If several packages of cycles with different amplitudes have to be handled (Fig. 2), each package demands an implicit calculation of the average stress change and the first cycle, followed by an explicit phase for the calculation with the HCA model.

In FE simulations with the HCA model the explicit phase can optionally be interrupted by so-called control cycles, which are again calculated implicitly in order to update the field of the strain amplitude. Usually such control cycles are introduced in logarithmic intervals (i.e., at N = 10, 100, 1000, etc). Since the effect of such control cycles on the cumulative settlements of shallow foundations was found to be of minor importance in earlier FE simulations (Wichtmann, 2005), control cycles have not been considered as an option in the sublayering model.

Validation and Parametric Studies

The sublayering model has been implemented as a Visual Basic for Applications (VBA) program for Microsoft Excel (Häcker, 2013; Wöhrle, 2012). The prediction has been checked against FE simulations with the HCA model using the finite element analysis (FEA) code Abaqus.

The calculations in Fig. 5 have been performed with an infinite distributed load applied on the ground surface. In both calculations, using either FE or the sublayering model, the same elastic stiffness approaches have been applied. For the first loading to the maximum stress, an equation derived from oedometric tests on Karlsruhe fine sand (KFS) (mean grain size d_{50} = 0.14 mm, uniformity coefficient C_u = 1.5, sample size d = 100 mm, h = 18 mm) has been used:

$$M\text{ [MPa]} = (0.29+0.49\cdot {I_D}^{1.14})(\sigma_1\text{ [kPa]})^{0.75} \quad (18)$$

with oedometric modulus M and vertical stress σ_1. The stiffness for the subsequent unloading to the average stress has been derived from the unloading curve measured in the same oedometric tests:

$$M_{ur}\text{ [MPa]} = 1.88\cdot(\sigma_1\text{ [kPa]})^{0.71} \quad (19)$$

Constant	c_{1a}	c_{1b}	c_2	c_3	c_4	c_5
Value	89.5	71.5	1143	4.33	0.60	0.20

Table 2 Material constants of Equations 20 to 25 for Karlsruhe fine sand

In both cases a Poisson's ratio ν = 0.3 has been applied. The strain amplitude as an input of the HCA model has been estimated based on a set of equations for the secant shear modulus G_{sec} obtained from drained cyclic triaxial tests performed in order to determine the HCA model parameters (see also Fig. 15). The secant shear modulus $G_{\text{sec}} = q^{\text{ampl}}/(3\varepsilon_q^{\text{ampl}})$ derived from the experimental data is plotted versus strain amplitude $\varepsilon^{\text{ampl}}$, void ratio e, average mean pressure p^{av}, and average stress ratio η^{av} in Fig. 4. The G_{sec} data in Fig. 4 are described by the following equations:

$$G_{\text{sec}} = c_{1a}\, f_{e,G}\, f_{p,G}\, f_{\eta,G}\, f_{\text{ampl},G} \tag{20}$$

$$f_{\text{ampl},G} = \frac{1}{1 + c_2\, \varepsilon^{\text{ampl}}/\sqrt{p/p_{\text{atm}}}} \tag{21}$$

$$f_{e,G} = \frac{(c_3 - e)^2}{1 + e} \tag{22}$$

$$f_{p,G} = {p_{\text{atm}}}^{1-c_4}\, (p^{\text{av}})^{c_4} \tag{23}$$

$$f_{\eta,G} = 1 + c_5(\eta^{\text{av}} - 0.75) \tag{24}$$

with p_{atm} = 100 kPa and the constants c_{1a} to c_5 summarized in Table 2. The functions $f_{\text{ampl},G}$, $f_{e,G}$, $f_{p,G}$, and $f_{\eta,G}$ with their constants c_2, c_3, c_4, and c_5 describe the decrease of the secant shear stiffness with strain amplitude and void ratio and its increase with average mean pressure and average stress ratio (Fig. 4). The parameter c_{1a} determines the overall magnitude of G_{sec}. Since $\varepsilon^{\text{ampl}}$ enters the equation for $f_{\text{ampl},G}$, the solution has to be done by iteration. If the amplitude dependence (Fig. 4a) is neglected for reasons of simplicity, one can use

$$G_{\text{sec}} = c_{1b}\, f_{e,G}\, f_{p,G}\, f_{\eta,G} \tag{25}$$

with another material constant c_{1b} (Table 2). Poisson's ratio ν = 0.26 has been derived from the same cyclic test data using $\nu = (3K_{\text{sec}} - 2G_{\text{sec}})/(6K_{\text{sec}} + 2G_{\text{sec}})$ with secant bulk modulus $K_{\text{sec}} = p^{\text{ampl}}/\varepsilon_v^{\text{ampl}} = q^{\text{ampl}}/(3\varepsilon_v^{\text{ampl}})$.

For the calculations with the sublayering model, the soil has been divided into 100 sublayers of equal height (0.5 m). The discretization used in the FE simulations is given in Fig. 7. Comparing the FE results with the prediction of the sublayering model, there are hardly any differences in the load-settlement curves during the application of the average load and the first cycle (not shown in Fig. 5). Additionally, the profiles of strain amplitude with depth are almost identical (Fig. 5a). The slightly larger cumulative settlements computed by the sublayering model (Fig. 5b) are due to the fact that the moderate increase of the lateral stress during the high cyclic loading (Fig. 5c), which leads to a somewhat stiffer response, is neglected in the sublayering model (i.e., $\dot{\sigma}_3$ = 0 instead of Eq. 16).

The comparison in Fig. 6 concerns a shallow strip foundation of width b = 10 m under cyclic loading. Hypoplasticity with intergranular strain and the parameters for Karlsruhe fine sand (Tables 3 and 4) have been applied for the monotonic loading and the first cycle in the FE simulation. The parameters in Tables 3 and 4 have been derived based on the same oedometric or cyclic triaxial tests that were used for the development of Eqs. 18-25. Therefore, the stiffness approaches used in the simulations with FE or the sublayering

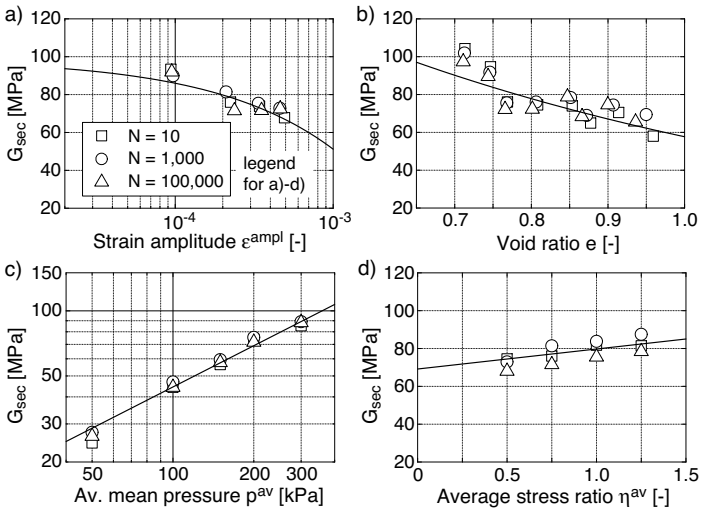

Fig. 4 Secant shear modulus G_{sec} derived from drained cyclic triaxial tests with different (a) stress and strain amplitudes, (b) initial void ratios, (c) average mean pressures, and (d) average stress ratios

φ_c [°]	h_s [MPa]	n [-]	α [-]	β [-]	e_{i0} [-]	e_{c0} [-]	e_{d0} [-]
33.1	2000	0.32	0.12	2.0	1.212	1.054	0.677

Table 3 Parameters of hypoplasticity for Karlsruhe fine sand

model are similar.

Figure 6 presents calculations with the sublayering model in which oedometric conditions (no lateral deformations, $\vartheta = 0$), biaxial conditions (free lateral deformations, $\vartheta = -\nu/2$), or mixed conditions (ϑ according to Eq. 4) have been used. Furthermore, the stiffness degradation of the secant stiffness has been considered (Eq. 20) or neglected (Eq. 25). Figure 6c clearly demonstrates that the cumulative settlement predicted by the sublayering model is larger for the triaxial case than for the mixed or oedometric conditions. Furthermore, considering the stiffness degradation leads to larger accumulated deformations. Compared to the FE results, the strain amplitude is overestimated by the sublayering model near the ground surface but slightly underestimated in larger depths (Fig. 6b). The latter is due to the fact that the stress amplitudes received from the FE simulations at larger depths exceeded those calculated in the sublayering model using Steinbrenner's formula. The discrepancies in the $\varepsilon^{\text{ampl}}$ values near the ground surface may have several causes. In the FE simulations the strain amplitude also changes in the horizontal direction (see the $\varepsilon^{\text{ampl}}$ field in Fig. 7). Larger $\varepsilon^{\text{ampl}}$ values at the ground surface are obtained near the edge of the foundation (compare the solid and dot-dashed green curves in Fig. 6b). Furthermore, the FE simulations show a compaction of the soil in the horizontal direction directly beneath the foundation, while a lat-

R [-]	m_R [-]	m_T [-]	β_R [-]	χ [-]
10^{-4}	2.6	1.3	0.1	6.0

Table 4 Parameters of intergranular strain for Karlsruhe fine sand

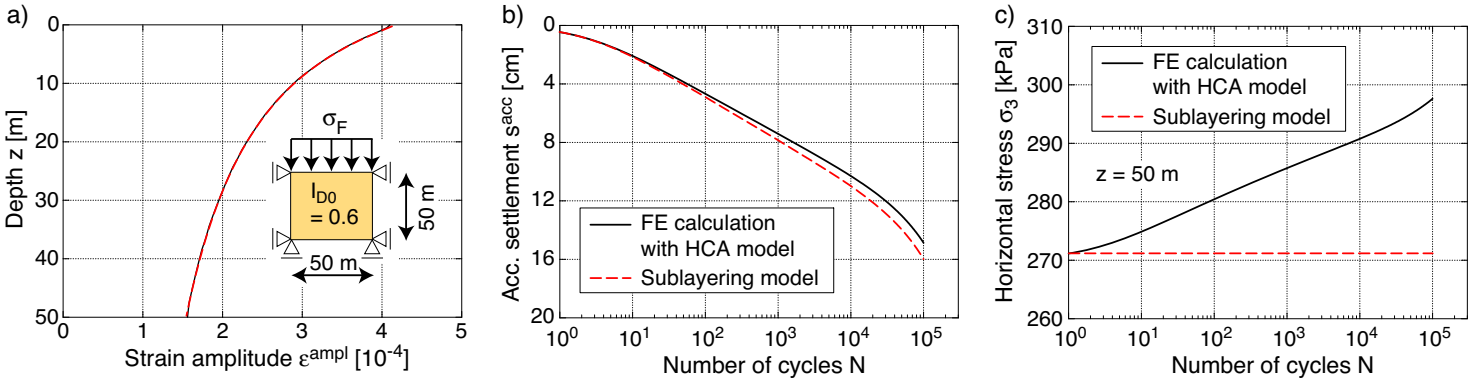

Fig. 5 Comparison of (a) strain amplitudes $\varepsilon^{\text{ampl}}(z)$, (b) accumulated settlement curves $s^{\text{acc}}(N)$, and (c) horizontal effective stress evolutions $\sigma_3(N)$ between FE calculations and simulations with the sublayering model for a cyclic loading with σ_F^{av} = 100 kPa and σ_F^{ampl} = 50 kPa applied as infinite distributed load on the ground surface (initial relative density of the soil I_{D0} = 0.6)

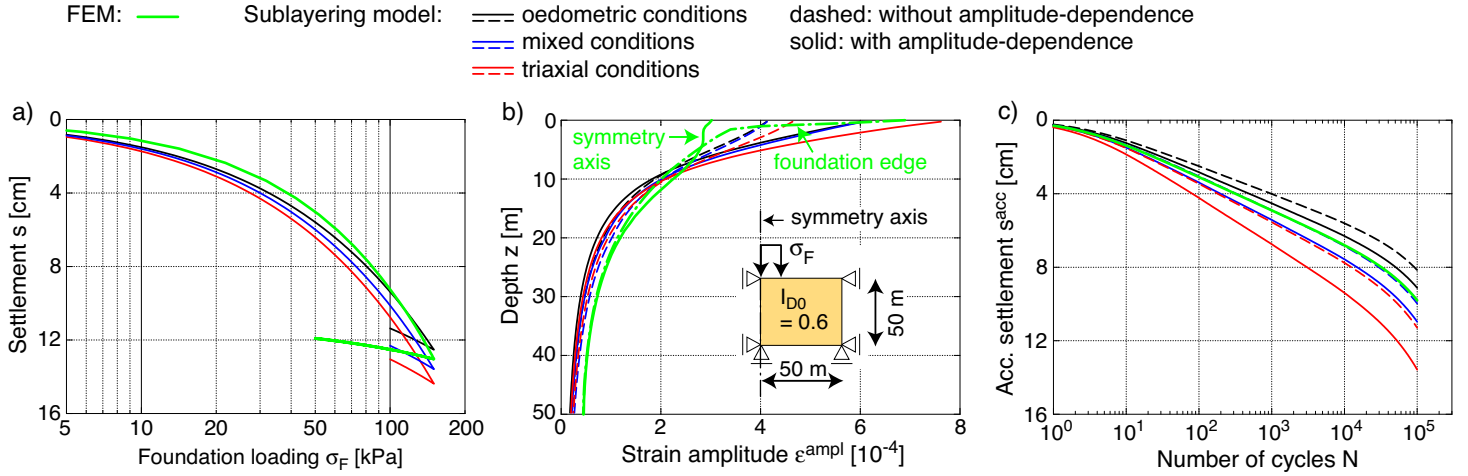

Fig. 6 Comparison of (a) load-settlement curves during the implicit phases of the calculation, (b) strain amplitudes $\varepsilon^{\text{ampl}}(z)$ below the center of the foundation, and (c) accumulated settlement curves $s^{\text{acc}}(N)$ between FE calculations and simulations with the sublayering model for cyclic loading with σ_F^{av} = 100 kPa and σ_F^{ampl} = 50 kPa applied on a foundation with width b = 10 m on medium dense sand (I_{D0} = 0.6)

eral extension increasing with depth is assumed in the sublayering model (Fig. 3). Differences in the constitutive description of the secant stiffness (Eqs. 20-25 in the sublayering model versus the intergranular strain concept in the FE simulations) and in the discretization of the soil (FE mesh versus 100 sublayers) may have contributed to the differences in the $\varepsilon^{\text{ampl}}(z)$ profiles. Because of the larger $\varepsilon^{\text{ampl}}$ values, the sublayering model predicts larger cumulative settlements in the upper part of the subsoil, while smaller ones are obtained at lower depths. These discrepancies almost compensate for each other since the curves of accumulated settlement $s^{\text{acc}}(N)$ from the FE calculations and the sublayering model agree well, in particular for the most realistic mixed boundary conditions (Fig. 6c).

The sublayering model is very useful for parametric studies since the effect of different parameters on the cumulative settlements can be quickly investigated. Figure 8 presents an example wherein the soil density, load amplitude, and dimensions and rigidity of a strip foundation have been varied. The sublayering model is also suitable for calculations with packages of cycles, as shown in Fig. 9 (obeying Miner's rule, i.e., the sequence of the amplitudes is of no importance), or with a stratified ground considering a dif-

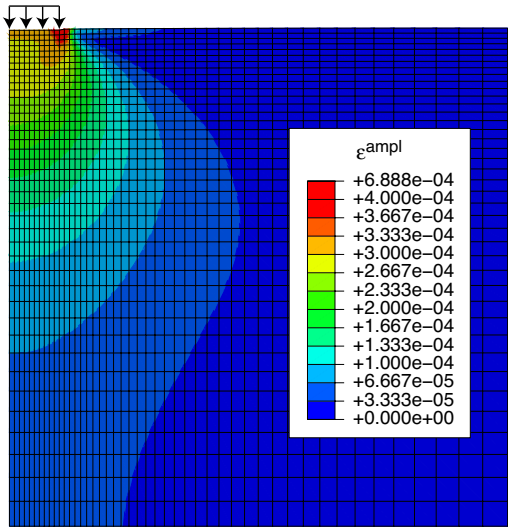

Fig. 7 FE mesh with field of strain amplitude $\varepsilon^{\text{ampl}}$ obtained in the calculation shown in Fig. 6

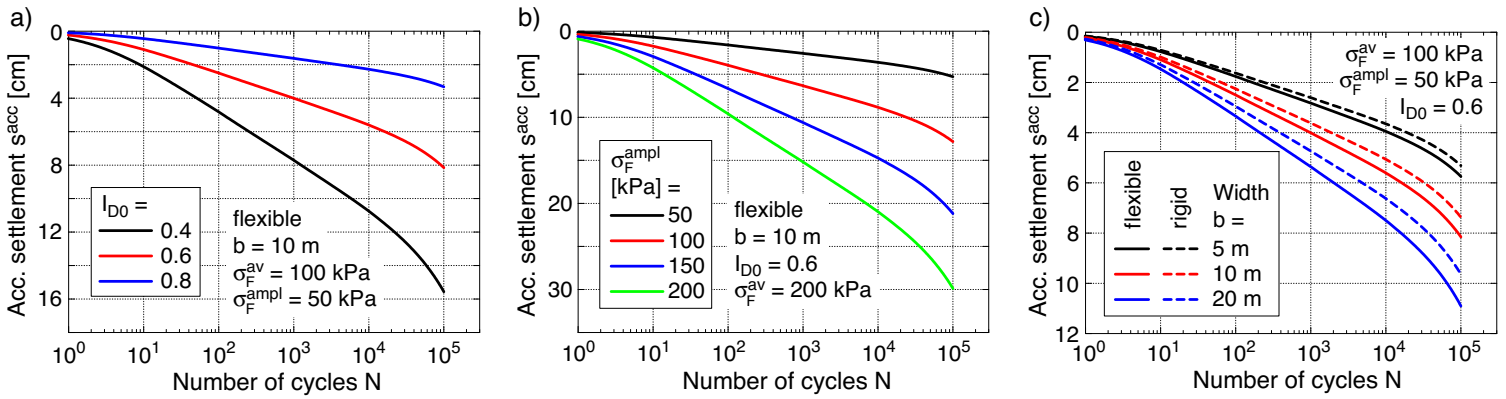

Fig. 8 Parametric study performed with the sublayering model: Accumulated settlement $s^{acc}(N)$ of a strip foundation in dependence on (a) relative density, (b) stress amplitude, and (c) width and rigidity of the foundation (all simulations with oedometric conditions, $\vartheta = 0$)

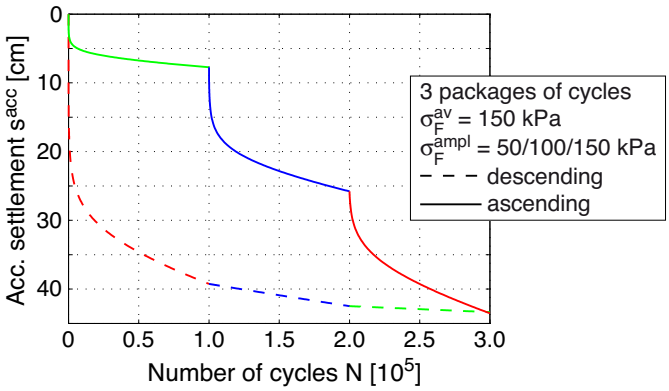

Fig. 9 Development of residual settlements predicted by the sublayering model during three packages of cycles with ascending or descending order of the amplitudes at constant average loading of the foundation

ferent cumulative response of the various layers.

HCA-BASED ENGINEER-ORIENTED MODELS FOR MONOPILES

Comparison of the HCA Prediction with Engineer-Oriented Models from the Literature

Westermann et al. (2014a,b) have compared various models for OWPP monopile foundations proposed in the literature (Achmus et al., 2008; American Petroleum Institute, 2000; Dührkop, 2010; Taşan, 2012) with the HCA model prediction using full 3-D FE simulations (see the FE model in Fig. 10). A monopile with an outer diameter of 5 m and a depth of embedding of 30 m has been studied under fully drained conditions. The simulations with the HCA model have been performed without control cycles (see remarks above) since preliminary FE calculations had not shown any significant influence on the long-term deformations of the monopile. Figure 11 compares the lateral deflections predicted by the various models after the first monotonic loading to the maximum loads (upper row of diagrams) and after 10^5 cycles (lower row) for three different loading conditions. Evidently, the predictions made by the five models differ significantly, although the parameters have been determined for the same sand (Karlsruhe fine sand), partially even from the same laboratory tests. The smallest horizontal deformations are obtained from the equations of the American Petroleum Institute (2000), followed by the approach of Dührkop (2010). In most cases, the largest deflections stem from the simulations with the ESWM (Taşan, 2012). It should be stressed that none of the models can be said to deliver the "right"prediction, since no data from in situ measurements or 1:1 model tests on monopile foundations are available yet that could serve as a validation of these models. As outlined by Zachert et al. (2016), the HCA model has at least been validated based on model tests on different scales and based on a full-scale in situ test on a shallow foundation for OWPPs.

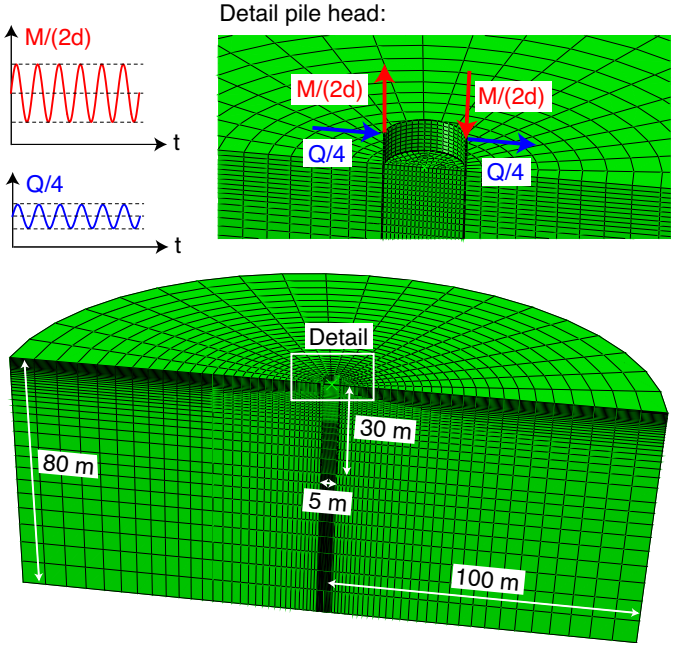

Fig. 10 FE model of an OWPP monopile foundation

In the following subsections, two different engineer-oriented models for OWPP monopile foundations based on the HCA model are presented. Their results are compared to those from full 3-D FE simulations using the model shown in Fig. 10.

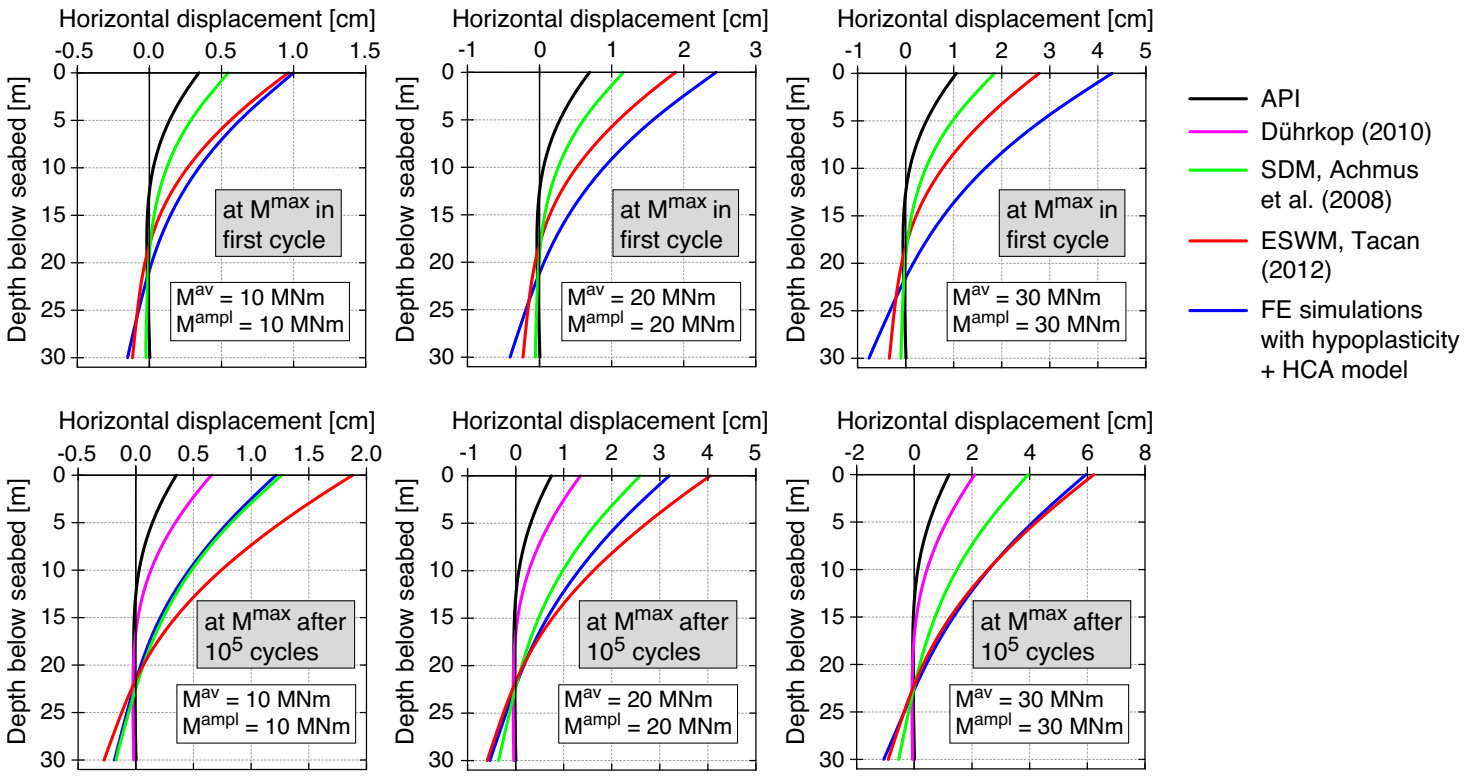

Fig. 11 Comparison of the pile deflections of an OWPP monopile foundation predicted by various models at maximum load ($M^{\max}$, $Q^{\max}$) in the first cycle (upper row) and after 10^5 load repetitions (lower row). Pile diameter = 5 m, depth of embedding = 30 m, initial relative density of the soil I_{D0} = 0.6, lever arm $h = M/V$ = 20 m (modified from Westermann et al. (2014b))

Sublayering Model

The monotonic and cumulative deformations are described by pairs of springs and dashpots in this model, arranged on either both sides or one side of the beam. Within this paper only the one-sided version (Fig. 12) is applied. A detailed description is given by Triantafyllidis and Chrisopoulos (2016).

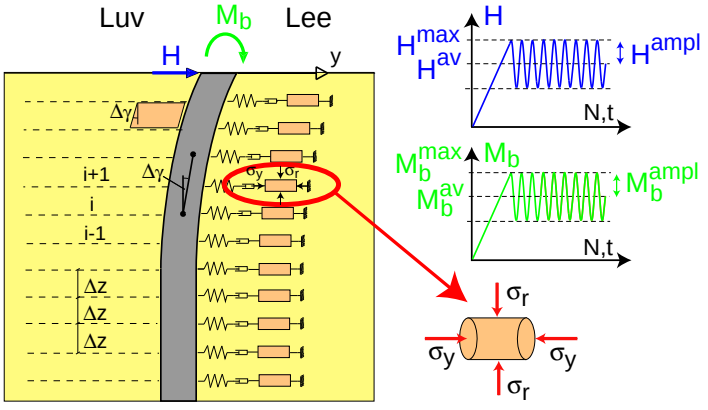

Fig. 12 Sublayering model with springs and dashpots arranged only on one side of the OWPP monopile foundation

The horizontal displacement y due to a static horizontal load H and a bending moment M_b applied at the top of the pile is obtained by solving the fourth-order differential equation of the beam-on-elastic foundation problem

$$EI \cdot \frac{d^4y}{dz^4} + K_s(z) \cdot y \cdot D = 0 \tag{26}$$

with the flexural stiffness EI of the pile, pile diameter D, bedding modulus K_s, and vertical coordinate z (z = 0 refers to the seabed). The bedding modulus $K_s = M/D$ is evaluated with the pile diameter D for $D \leq 1$ m and with D = 1 m for $D > 1$ m (this restriction has been overtaken from DIN 1054-2005; DIN (2005)). The oedometric modulus M is calculated from $M = \frac{1+e_0}{C_c}\sigma'_y$ for loading and $M = \frac{1+e_0}{C_s}\sigma'_y$ for un- and reloading. Therein C_c and C_s are the compression or swelling indices from oedometric tests, σ'_y is the initial horizontal stress (K_0 stress conditions), and e_0 is the initial void ratio. The following boundary conditions are used for the solution:

$$z = 0: \qquad EI \cdot \frac{d^2y}{dz^2} = M_b \qquad EI \cdot \frac{d^3y}{dz^3} = H \tag{27}$$

$$z = L: \qquad EI \cdot \frac{d^2y}{dz^2} = 0 \qquad EI \cdot \frac{d^3y}{dz^3} = 0 \tag{28}$$

with L being the depth of embedding of the pile. For the fine sand considered in this paper (Karlsruhe fine sand), $C_c = 0.0131 - 0.0095 \cdot I_D$ and $C_s = 0.0044 - 0.0017 \cdot I_D$ have been applied based on oedometric tests with a variation of initial relative density I_D.

Next, the deformations due to the cyclic loading are treated with equations based on the HCA model. The increment of horizontal

displacement Δy_i^{Pile} of the pile is coupled with the unknown increment of stress $\Delta\sigma_i$ (the index $\sqcup_i$ numbers the support points or layers, respectively) in the soil caused by the cycles via

$$[\mathbf{K}] \cdot \left[\Delta y_i^{\text{Pile}}\right] = [(-\Delta\sigma_i) \cdot \Delta z \cdot L_c] \tag{29}$$

Therein $\mathbf{K}$ is the stiffness matrix of the beam, $L_c = \pi D/4$ is a characteristic length in the horizontal direction, and Δz is the distance between two springs or dashpots in the vertical direction (Fig. 12). A constant value of Δz = 1 m is used herein. The displacement of the pile is assumed to be identical to that of the soil; i.e., $\Delta y_i^{\text{Pile}} = \Delta y_i$. The increment of shear strain $\Delta\gamma_i$ in the soil next to the pile is expressed by means of the increments of displacement of the adjacent support points (Fig. 12):

$$\Delta\gamma_i = \frac{\Delta y_{i+1}^{\text{Pile}} - \Delta y_{i-1}^{\text{Pile}}}{2\Delta z} \tag{30}$$

As illustrated in Fig. 12, triaxial conditions are assumed for each layer. The increment of stress in the soil $\Delta\sigma_i$ is thus obtained from

$$\Delta\sigma_i = \Delta p_i + \frac{2}{3}\Delta q_i \tag{31}$$

using

$$\Delta p_i^1 = K(p_i^0) \cdot \left[\frac{2}{3}\left(\Delta\gamma_i^1 \cdot \frac{m_v^0}{m_q^0}\right) - m_v^0 \cdot \Delta\varepsilon_i^{\text{acc},0} - m_v^0 \cdot \frac{2}{3\sqrt{3}}\, Y^0 \cdot \Delta\gamma_i^1\right] \tag{32}$$

$$\Delta q_i^1 = 3G(p_i^0) \cdot \left[\frac{2}{3} \cdot \Delta\gamma_i^1 - m_q^0 \cdot \Delta\varepsilon_i^{\text{acc},0} - \sqrt{\frac{2}{3}} \cdot Y^0 \cdot m_q^0 \cdot \Delta\gamma_i^1\right] \tag{33}$$

with K (bulk modulus) and G (shear modulus) being the components of the stiffness used in the HCA model. m_v and m_q are the components of the HCA flow rule (Eq. 11) written in terms of Roscoe's invariants. The indices $\sqcup^0$ and $\sqcup^1$ in Eqs. 32 and 33 denote the states at the start and the end of an increment. The stress ratio is Y = 1 for $\eta/M \geq 1$ and Y = 0 for $\eta/M < 0$.

The sublayering model has been implemented using the program Wolfram Mathematica. Simulation results are discussed in a later subsection.

SDM Based on HCA (HCA-SDM)

The second model for monopiles is a stiffness-degradation approach similar to that proposed by Achmus et al. (2008) but based on the equations of the HCA model. It is called HCA-SDM in the following. In Fig. 13 the calculation scheme of the HCA-SDM is confronted with the real stress–strain behaviour under cyclic loading. The procedure consists of two successive FE calculations with an elastoplastic model. The first calculation includes the loading to the minimum load $\sigma^{\min}$ (point 1 in Fig. 13b), the loading to the maximum load $\sigma^{\max}$ (point 2), the unloading to $\sigma^{\min}$ (point 3), and the final reloading to the average stress σ^{av} (point 4). For the initial phase up to point 2, a pressure- and density-dependent elastic stiffness for first loading (e.g., C_c from oedometric tests or E_{50} from triaxial tests) is applied, while a stiffness for un- and reloading (C_s, E_{ur}) is needed for the rest of the calculation. The strains computed at points 2-4 are saved in state variables. They are further used to calculate the stiffness-degradation factor r for the maximum number of cycles $N_{\max}$ under consideration. In the subsequent second calculation, starting from point 1, the monotonic loading to the maximum load (points 2-6 in Fig. 13b) is calculated with Young's modulus for first loading reduced by the factor r. The larger strains resulting from this reduction of stiffness are thought to incorporate the accumulated strains due to $N_{\max}$ cycles.

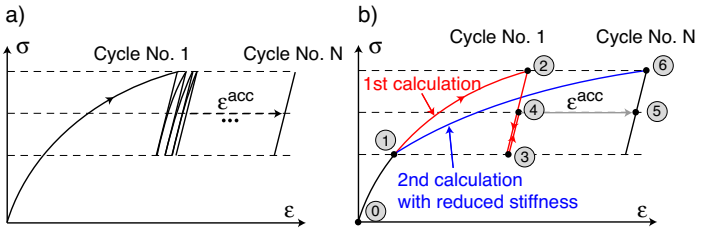

Fig. 13 (a) Real stress-strain behavior under cyclic loading, (b) calculation scheme of HCA-SDM

To derive a formulation for r based on the HCA model, the difference of the strains at points i and j is denoted as $\boldsymbol{\varepsilon}^{i-j} = \boldsymbol{\varepsilon}^j - \boldsymbol{\varepsilon}^i$ and its norm is noted as $\varepsilon^{i-j} = \|\boldsymbol{\varepsilon}^j - \boldsymbol{\varepsilon}^i\|$. The strain at the maximum load after $N_{\max}$ cycles is $\boldsymbol{\varepsilon}^{1-6} = \boldsymbol{\varepsilon}^{1-2} + \boldsymbol{\varepsilon}^{2-4} + \boldsymbol{\varepsilon}^{4-5} + \boldsymbol{\varepsilon}^{5-6}$. With $\boldsymbol{\varepsilon}^{2-4} = -\boldsymbol{\varepsilon}^{5-6}$ one obtains $\boldsymbol{\varepsilon}^{1-6} = \boldsymbol{\varepsilon}^{1-2} + \boldsymbol{\varepsilon}^{4-5}$. Assuming coaxiality between the strains $\boldsymbol{\varepsilon}^{1-2}$ resulting from monotonic loading and the cumulative portion $\boldsymbol{\varepsilon}^{4-5}$, one gets $\varepsilon^{1-6} = \varepsilon^{1-2} + \varepsilon^{4-5} = \varepsilon^{1-2} + \varepsilon^{\text{acc}}$. The stiffness-degradation factor can then be derived from

$$r = \frac{\varepsilon^{1-2}}{\varepsilon^{1-6}} = \frac{\varepsilon^{1-2}}{\varepsilon^{1-2} + \varepsilon^{\text{acc}}} \tag{34}$$

While ε^{1-2} is known from the first calculation, the accumulated strain is evaluated from $\varepsilon^{\text{acc}} = f_{\text{ampl}} f_N f_e f_p f_Y$ with $N_{\max}$ entering f_N and with the average stresses (p^{av}, η^{av}) and void ratios (e^{av}) at point 4. The strain amplitude is computed from $\varepsilon^{\text{ampl}} = \frac{1}{2}\|\boldsymbol{\varepsilon}^2 - \boldsymbol{\varepsilon}^3\| = \frac{1}{2}\varepsilon^{2-3}$. The strain ε^{2-3} is also available from the first calculation.

Validation

The deformations for a monopile after 10^5 cycles as given in Fig. 11 have been simulated with both HCA-based engineer-oriented models. The results for three different loading conditions are presented in Fig. 14. Evidently, the deflection curves obtained from the sublayering model lie close to the results from the full FE simulations with the HCA model. The deformations computed with the HCA-SDM are, however, much larger. This is mainly due to the fact that, in the simulations with the full HCA model, a strain accumulation occurs on both sides of the pile. The cumulative strains on the lee side lead to an increase of the pile tilting, while this process is counteracted by the strains on the windward side. In the case of the HCA-SDM, owing to the "calculation trick"of applying a reduced stiffness, the weakened soil on the lee side determines the pile deformations, while the softer soil on the windward side is of minor importance. A comparison of Fig. 14 with the lower row of diagrams in Fig. 11 reveals that the deflections obtained with the HCA-SDM exceed the permanent deformations predicted by all other models applied in the comparative study documented in Westermann et al. (2014a,b). Therefore, it may be concluded that the HCA-SDM gives results being too conservative.

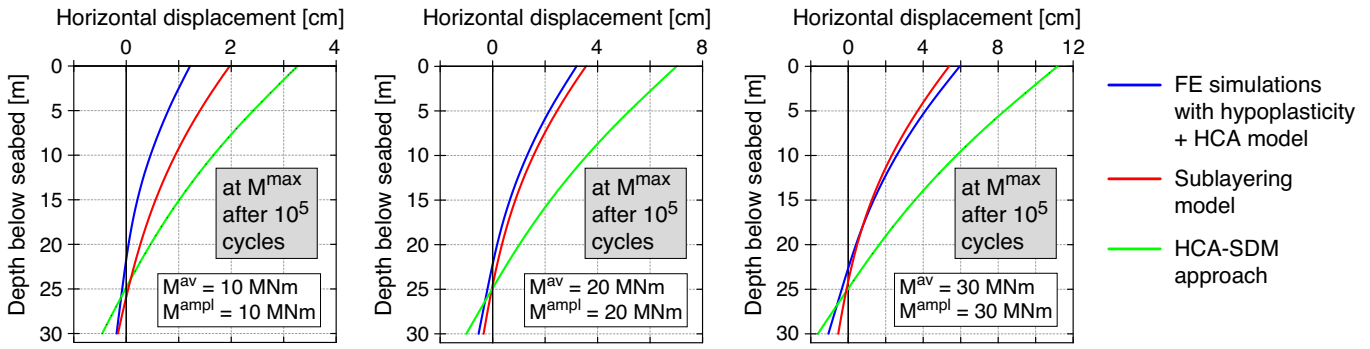

Fig. 14 Lateral deflections of the monopile predicted with the engineer-oriented models based on the HCA model compared to FE simulations with the full HCA model (pile diameter = 5 m, depth of embedding = 30 m, initial relative density of the soil I_{D0} = 0.6, lever arm $h = M/V$ = 20 m)

SIMPLIFIED CALIBRATION OF HCA MODEL PARAMETERS

The determination of the HCA model parameters C_{ampl}, C_e, C_p, C_Y, C_{N1}, C_{N2}, and C_{N3} (Table 1) from drained cyclic triaxial tests is quite laborious. At least 11 tests with different stress amplitudes q^{ampl}, initial relative densities I_{D0} of the soil samples, average mean pressures p^{av}, and average stress ratios η^{av} are necessary. Figure 15 presents an example of the results of such test series in terms of the development of accumulated strain ε^{acc} with increasing number of cycles N. The data in Figure 15 reveal that the intensity of strain accumulation grows with increasing values of amplitude and stress ratio while it decreases if the sand becomes denser. The strain accumulation curves measured for the different average mean pressures are similar if the amplitude-pressure ratio $q^{\text{ampl}}/p^{\text{av}}$ is kept constant. The parameters C_{ampl}, C_e, C_p, and C_Y are obtained based on the $\varepsilon^{\text{acc}}(N)$ curves from the test series with different values of q^{ampl}, I_{D0}, p^{av}, and η^{av}. Afterward, the data of all tests are utilized to determine the remaining three parameters C_{N1}, C_{N2}, and C_{N3}, which describe the shape of the strain accumulation curves. Finally the tests can be recalculated with the HCA model (see blue curves in Fig. 15) in order to check the prediction quality or to optimize the parameters. A more detailed description of the procedure for a calibration of the HCA model parameters based on cyclic test data is provided in (Wichtmann, 2016; Wichtmann et al., 2010b, 2015).

To reduce the effort for the calibration, a simplified procedure has been developed. It uses correlations between the HCA model parameters and characteristic values of the grain size distribution curve (mean grain size d_{50}, uniformity coefficient C_u) or index properties (minimum void ratio $e_{\min}$) that can be easily determined in the laboratory. Based on the data from approximately 350 drained cyclic triaxial tests on 22 clean quartz sands with different grain size distribution curves and subangular grain shape, the following equations have been proposed by Wichtmann et al. (2015):

$$C_{\text{ampl}} = 1.70 \tag{35}$$

$$C_e = 0.95 \cdot e_{\min} \tag{36}$$

$$C_p = 0.41 \cdot [1 - 0.34\ (d_{50}[\text{mm}] - 0.6)] \tag{37}$$

$$C_Y = 2.60 \cdot [1 + 0.12\ \ln(d_{50}[\text{mm}]/0.6)] \tag{38}$$

$$C_{N1} = 4.5 \cdot 10^{-4} \cdot [1 - 0.306\ \ln(d_{50}[\text{mm}]/0.6)] \cdot [1 + 3.15\ (C_u - 1.5)] \tag{39}$$

$$C_{N2} = 0.31 \cdot \exp[0.39\ (d_{50}[\text{mm}] - 0.6)] \cdot \exp[12.3(\exp(-0.77 C_u) - 0.315)] \tag{40}$$

$$C_{N3} = 3.0 \cdot 10^{-5} \cdot \exp[-0.84\ (d_{50}[\text{mm}] - 0.6)] \cdot [1 + 7.85\ (C_u - 1.5)]^{0.34} \tag{41}$$

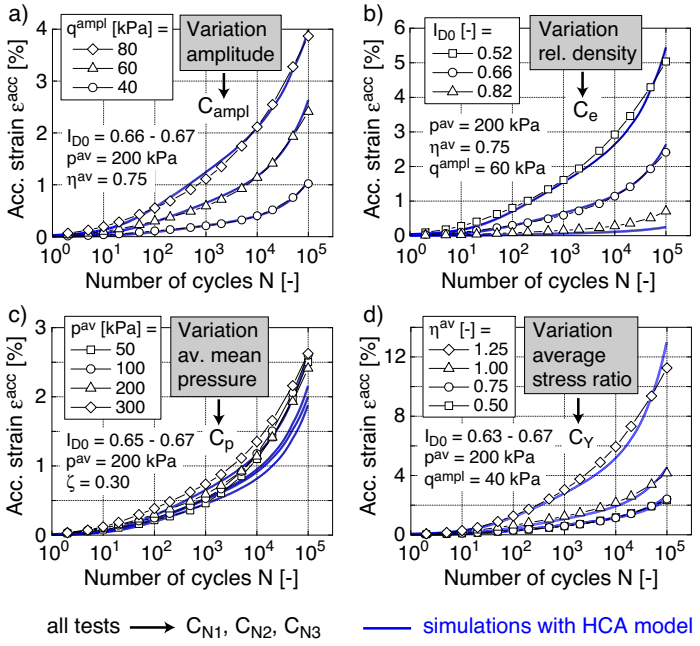

Fig. 15 Determination of the parameters C_{ampl}, C_e, C_p, C_Y, C_{N1}, C_{N2}, and C_{N3} of the HCA model from the strain accumulation curves $\varepsilon^{\text{acc}}(N)$ measured in four series of drained cyclic tests with different (a) stress amplitudes, (b) relative densities, (c) average mean pressures, and (d) average stress ratios (amplitude–pressure ratio $\zeta = q^{\text{ampl}}/p_0$)

The HCA model parameters can be completely or partially estimated from Eqs. 35-41. For example, the parameters C_{ampl}, C_e, C_p, and C_Y are obtained from Eqs. 35-38, while C_{N1}, C_{N2}, and C_{N3} are determined from a single cyclic test. Such mixed calibration based on a single test may be regarded as a minimum requirement. A determination of all parameters by means of Eqs. 35-41 should be restricted to rough estimations only, since the equations do not consider the influence of grain shape or fines content yet. The accuracy of predictions using sets of parameters calibrated either from numerous cyclic tests or from a single cyclic test or from Eqs. 35-41 has been discussed by Wichtmann et al. (2015) and Zachert et al. (2015).

CONCLUSIONS

Several engineer-oriented models dedicated to the prediction of permanent deformations of OWPP foundations under high cyclic loading have been presented. They are all based on the HCA model proposed by Niemunis et al. (2005). For shallow foundations under vertical cyclic loading, a sublayering model has been developed in analogy to the conventional calculation of settlements caused by monotonic loading. The sublayering model reproduces well the cumulative settlements obtained from FE simulations using the full HCA model. For monopiles, two different approaches have been compared: a sublayering model and a stiffness-degradation approach. While the cumulative horizontal displacements of the sublayering model agree well with 3-D FE simulations, the stiffness-degradation approach overestimates the deformations, i.e. this approach is too conservative. The sublayering model, however, seems suitable for application to OWPP monopile foundations. Furthermore, a simplified procedure for the calibration of the HCA model constants has been briefly outlined.

ACKNOWLEDGEMENTS

The authors are grateful for the financial support of the Federal Ministry for the Environment, Nature Conversation and Nuclear Safety (BMU) under research grants 0325175 and 0325405A/B.

REFERENCES

DIN 1054:2005. Baugrund; Sicherheitsnachweise im Erd und Grundbau, 2005.

M. Achmus, Y.-S. Kuo, and A. Abdel-Rahman. Zur Bemessung von Monopiles für zyklische Lasten. *Der Bauingenieur*, 83:303–311, 2008.

API American Petroleum Institute. Recommended practice for planning, designing and constructing fixed offshore platforms - Working stress design. API RP 2A - WSD, Washington CD, USA, 2000.

M. Ashour, G. Norris, and P. Pilling. Lateral loading of a pile in layered soil using the strain wedge model. *Journal of Geotechnical and Geoenvironmental Engineering, ASCE*, 124(4):303–315, 1998.

V.A. Diyaljee and G.P. Raymond. Repetitive load deformation of cohesionless soil. *Journal of the Geotechnical Engineering Division, ASCE*, 108(GT10):1215–1229, 1982.

J. Dührkop. Zum Einfluss von Aufweitungen und zyklischen Lasten auf das Verformungsverhalten lateral beanspruchter Pfähle in Sand. Dissertation, Veröffentlichungen des Institutes für Geotechnik und Baubetrieb der Technischen Universität Hamburg-Harburg, Heft Nr. 20, 2010.

A. Häcker. Erweiterung eines Lamellenmodells für zyklisch belastete Flachgründungen. Diplomarbeit, Institut für Bodenmechanik und Felsmechanik, Karlsruher Institut für Technologie (KIT), 2013.

U. Hartwig. Planung der versuchstechnischen Simulation des Verhaltens einer Flachgründung für Offshore-Windenergieanlagen im Originalmaßstab. In *Workshop "Gründung von Offshore-Windenergieanlagen", Karlsruhe 2010, Veröffentlichungen des Institutes für Bodenmechanik und Felsmechanik am Karlsruher Institut für Technologie (KIT), Heft Nr. 172*, pages 81–97, 2010.

A. Hettler. Verschiebungen von lotrecht mittig belasteten Einzelfundamenten und horizontal belasteten Pfählen in Sand unter Schwellast. *Der Bauingenieur*, 59:351–355, 1984.

C. Leblanc, G.T. Houlsby, and B.W. Byrne. Response of stiff piles in sand to long-term cyclic lateral loading. *Géotechnique*, 60(2):79–90, 2010.

K. Mallwitz and U. Holzlöhner. Verfahren zur Ermittlung der Setzung von Fundamenten infolge zyklischer Beanspruchung. *Bautechnik*, 73 (3):175–186, 1996.

A. Niemunis and T. Wichtmann. Separation of time scale in the HCA model for sand. *Acta Geophysica*, 62(5):1127–1145, 2014.

A. Niemunis, T. Wichtmann, and Th. Triantafyllidis. A high-cycle accumulation model for sand. *Computers and Geotechnics*, 32(4):245–263, 2005.

G.M. Norris. Theoretically based BEF laterally loaded pile analysis. In *Proc. 3rd Int. Conf on Numerical Methods in Offshore Piling, Nantes, France*, pages 361–386, 1986.

K. Nübel, Ch. Karcher, and I. Herle. Ein einfaches Konzept zur Abschätzung von Setzungen. *Geotechnik*, 22(4):251–258, 1999.

H.E. Taşan. Prognose der Verschiebungen von zyklisch lateral belasteten Monopiles in geschichteten Böden. *Der Bauingenieur*, (6):297–305, 2012.

T. Triantafyllidis and S. Chrisopoulos. Ein Modell zur Berechnung des Verformungsverhaltens von horizontal hochzyklisch beanspruchten Pfählen. *Bautechnik*, 93(9):605–627, 2016.

K. Westermann, H. Zachert, and T. Wichtmann. Vergleich von Ansätzen zur Prognose der Langzeitverformungen von OWEA-Monopilegründungen in Sand. Teil 1: Grundlagen der Ansätze und Parameterkalibration. *Bautechnik*, 91(5):309–323, 2014a.

K. Westermann, H. Zachert, and T. Wichtmann. Vergleich von Ansätzen zur Prognose der Langzeitverformungen von OWEA-Monopilegründungen in Sand. Teil 2: Simulationen und Schlussfolgerungen. *Bautechnik*, 91(5):324–332, 2014b.

T. Wichtmann. Explicit accumulation model for non-cohesive soils under cyclic loading. PhD thesis, Publications of the Institute of Soil Mechanics and Foundation Engineering, Ruhr-University Bochum, Issue No. 38, 2005.

T. Wichtmann. Soil behaviour under cyclic loading - experimental observations, constitutive description and applications. Habilitation thesis, Publications of the Institute of Soil Mechanics and Rock Mechanics, Karlsruhe Institute of Technology, Issue No. 181, 2016.

T. Wichtmann, A. Niemunis, and Th. Triantafyllidis. Towards the FE prediction of permanent deformations of offshore wind power plant foundations using a high-cycle accumulation model. In *International Symposium: Frontiers in Offshore Geotechnics, Perth, Australia*, pages 635–640, 2010a.

T. Wichtmann, A. Niemunis, and Th. Triantafyllidis. On the determination of a set of material constants for a high-cycle accumulation model for non-cohesive soils. *International Journal For Numerical And Analytical Methods in Geomechanics*, 34(4):409–440, 2010b.

T. Wichtmann, A. Niemunis, and Th. Triantafyllidis. Improved simplified calibration procedure for a high-cycle accumulation model. *Soil Dynamics and Earthquake Engineering*, 70(3):118–132, 2015.

T. Wöhrle. Überprüfung und Weiterentwicklung einfacher Ingenieurmodelle für Offshore-Windenergieanlagen auf Basis des Akkumulationsmodells. Diplomarbeit, Institut für Bodenmechanik und Felsmechanik, Karlsruher Institut für Technologie (KIT), 2012.

H. Zachert. Zur Gebrauchstauglichkeit von Gründungen für Offshore-Windenergieanlagen. Dissertation, Veröffentlichungen des Institutes für Bodenmechanik und Felsmechanik am Karlsruher Institut für Technologie, Heft Nr. 180, 2015.

H. Zachert, T. Wichtmann, P. Kudella, T. Triantafyllidis, and U. Hartwig. Validation of a high cycle accumulation model via FE-simulations of a full-scale test on a gravity base foundation for offshore wind turbines. In *International Wind Engineering Conference, IWEC 2014, Hannover*, 2014.

H. Zachert, T. Wichtmann, T. Triantafyllidis, and U. Hartwig. Simulation of a full-scale test on a Gravity Base Foundation for Offshore Wind Turbines using a High Cycle Accumulation Model. In *3rd International Symposium on Frontiers in Offshore Geotechnics (ISFOG), Oslo*, 2015.

H. Zachert, T. Wichtmann, and Th. Triantafyllidis. Soil structure interaction of foundations for offshore wind turbines. In *26th International Ocean and Polar Engineering Conference (ISOPE-2016), Rhodos*, 2016.